Earth's Future

RESEARCH ARTICLE
10.1029/2018EF001103

Drought Occurring With Hot Extremes: Changes Under Future Climate Change on Loess Plateau, China

C. X. Sun[1], G. H. Huang[2], Y. Fan[3], X. Zhou[4], C. Lu[4], and X. Q. Wang[5]

[1]Key Laboratory of Regional Energy and Environmental Systems Optimization, Ministry of Education, North China Electric Power University, Beijing, China, [2]Center for Energy, Environment and Ecology Research, UR-BNU, Beijing Normal University, Beijing, China, [3]College of Engineering, Design and Physical Sciences, Brunel University, London, UK, [4]Faculty of Engineering and Applied Science, University of Regina, Regina, Saskatchewan, Canada, [5]School of Climate Change and Adaptation, University of Prince Edward Island, Charlottetown, Prince Edward Island, Canada

Key Points:
- A modeling system is developed to investigate future characteristics of simultaneous occurrence of drought and hot extremes
- Precipitation projections from PRICIS and RegCM models were jointly corrected by the multidimensional copula model
- Results show that some stations in partial area of Loess Plateau may experience hot droughts that are more frequent and extreme in future

Correspondence to:
G. H. Huang and Y. Fan,
huang@iseis.org;
yurui.fan@brunel.ac.uk

Citation:
Sun, C. X., Huang, G. H., Fan, Y., Zhou, X., Lu, C., & Wang, X. Q. (2019). Drought occurring with hot extremes: Changes under future climate change on Loess Plateau, China. *Earth's Future*, 7. https://doi.org/10.1029/2018EF001103

Received 12 NOV 2018
Accepted 23 APR 2019
Accepted article online 29 APR 2019

Abstract Drought is one of the most widespread and destructive hazards over the Loess Plateau (LP) of China. Due to climate change, extremely high temperature accompanied with drought (expressed as hot drought) may lead to intensive losses of both properties and human deaths in future. A hot drought probabilistic recognition system is developed to investigate how potential future climate changes will impact the simultaneous occurrence of drought and hot extremes (hot days exceeding certain values) on the LP. Two regional climate models, coupled with multiple bias-correction techniques and multivariate probabilistic inference, are innovative integrated into the hot drought probabilistic recognition system to reveal the concurrence risk of droughts and hot extremes under different Representative Concentration Pathway (RCP) scenarios. The hot-day index, TX90p, indicating the number of days with daily maximum temperature (T_{max}) exceeding the 90th percentile threshold, and the Standardized Precipitation Index are applied to identify the joint risks on the LP using copula-based methods. The results show that precipitation will increase throughout most of the LP under both RCP4.5 and RCP8.5 scenarios of 2036–2095, while T_{max} may increase significantly all over the LP (1.8–2.7 °C for RCP4.5 and 2.7–3.6 °C for RCP8.5). The joint return periods of Standardized Precipitation Index and TX90p show that fewer stations will experience severe drought with long-term hot extremes in two future scenarios. However, some stations may experience hot droughts that are more frequent and extreme, particularly certain stations in the southwest and south-central regions of the LP with recurrence period less than 10 years.

1. Introduction

Extreme climate events, such as drought and hot extremes, have been occurring on a wide range of time scales and in many parts of the world in relation to climate change (Bates et al., 2008; Mishra & Singh, 2010; von Buttlar et al., 2018). Heat waves cause water loss, lower the yield of agricultural products, increase energy consumption, and adversely affect human health in a variety of direct, indirect, immediate, and delayed ways (Mazdiyasni & Aghakouchak, 2015; U.S. Department of Energy, 2013; Zaitchik et al., 2006). Drought, characterized by less than normal precipitation over a period of months to years (Zhang & Zhou, 2015), has devastating impacts on the ecological environment and social-economic sectors, including the urban water supply, modern industries, and also the agricultural production (Food and Agricultural Organisation of United nations (FAO), 2002; Heim, 2002; von Buttlar et al., 2018; World Bank, 2003). Drought is one of the most expensive natural disasters and causes annual losses estimated at $6–8 billion in the United States (Keyantash & Dracup, 2002). Furthermore, drought-related disasters killed over half a million people in Africa during the 1980s (Kallis, 2008).

High temperatures and drought often interact with each other: a sustained precipitation deficit during summer plays an important role in intensifying subsequent extreme temperatures, and drought may also be triggered and aggravated by temperature extremes (Bandyopadhyay et al., 2016; Mueller & Seneviratne, 2012; Zaitchik et al., 2006). Drought can occur simultaneously with a heat wave, and concurrent events have been observed to cause a series of extreme effects on human and natural systems (Zscheischler & Seneviratne, 2017).

Occurring with a heat wave, the Great U.S. Drought of 2012 led to a damage cost more than $33 billion, which is the most extensive drought in the United States since the 1930s (NOAA, 2018). Furthermore, the associated summer heat wave caused 123 direct deaths (Masters, 2013; NOAA, 2018). It is thus vitally

important to analyze the correlations between concurrent droughts and heat waves (hot droughts) and determine their characteristics of simultaneous occurrence to enable water resource management planning and the development of adaptive strategies to mitigate the associated negative effects of climatic change.

No uniform definitions of drought currently exist, but many quantitative definitions and related indices have been proposed to accurately assess the drought severity for risk management (Burke et al., 2006). The Palmer Drought Severity Index, Standardized Precipitation Index (SPI), and the Standardized Precipitation Evapotranspiration Index are three of the most commonly used drought indexes, and they all have their own advantages and disadvantages (Dubrovsky et al., 2009; Guttman, 1998; Keyantash & Dracup, 2002; Vicente-Serrano et al., 2010). In this study, the SPI index which has been recommended by World Meteorological Organization is selected to quantify the degree of meteorological drought. The SPI is applied due to its strong ability in drought identification and assessment of drought grade (Mishra & Singh, 2010). This index is also one of the drought identification indicators recommended by China Meteorological Drought Classification Standard (National Climate Center, 2017) and has good performance in identifying meteorological drought on the Loess Plateau (see Huang et al., 2018; Liu et al., 2016; Wu et al., 2018; Xu et al., 2015). Based on precipitation projections from global climate models (GCMs) or regional climate models (RCMs), SPI is widely used to address future meteorological drought in many parts of the world (Asadi Zarch et al., 2015; Huang et al., 2018; Osuch et al., 2016; Vidal & Wade, 2009). Five temperature indices were applied by Mekis and Vincent (2006) to study extreme temperature; of these, we have applied the number of days with daily maximum temperature (T_{max}) exceeding the 90th percentile threshold (TX90p) in our study, in accordance with the World Meteorological Organization standards (Karl et al., 1999).

The Loess Plateau (LP) is located in the upper and middle reaches of the Yellow River and it is acknowledged to be an area suffering from severe soil erosion and a shortage of water resources. However, the LP is an important agricultural region in China, and its natural conditions (i.e., water shortage, serious soil erosion, and its different climatic regions) make it particularly important to assess its drought and high-temperature response to global climate changes (Zhang et al., 2012). Most past studies have focused on either drought or high temperatures, and few assessments have been made that combine these characteristics, particularly for the LP. However, some studies have simply identified the occurrence of drought or high temperatures and their spatial distribution, although they have not quantitatively expressed a joint probability recurrence period (Li et al., 2010; Liu et al., 2016; She & Xia, 2018). It has been predicted that the frequency and severity of extreme events may change in the future in relation to the effects of greenhouse gas emissions and global climate change (IPCC, 2007). Therefore, it is of considerable important to determine how future climate change in the Loess Plateau will affect drought and high temperatures, to ultimately develop improved adaptive strategies.

GCMs are commonly used to generate future climate projections under different Representative Concentration Pathway (RCPs; Wang et al., 2014). However, as GCMs are too coarse to assess regional or local scale climatic characteristics and may have large systematic biases, RCMs are usually employed to transform GCM outputs to a higher resolution prior to subsequent bias corrections (Wang et al., 2014; Zhou et al., 2017). Consequently, this study aims to establish a modeling system for investigating the potential future climate change impacts on hot droughts in the Loess Plateau. In detail, the PRECIS (Providing Regional Climates for Impacts Studies) and RegCM are used to simulate precipitation and T_{max} of historical and projected future (in both moderate (RCP 4.5) and high (RCP 8.5) future emissions scenarios) periods in the LP. After conducting a bias correction process, the commonly used quantile mapping method (Q_{map}) tool is used to correct the T_{max} bias, while a multidimensional copula model is developed to correct for monthly precipitation. After the implementation of statistical test, the selected marginal distributions and copulas are fitted to construct copula-based joint distributions of TX90p and SPI (SPI value for May to October). Finally, the performance of a single variable and bivariate return periods at different levels under different scenarios in the future is analyzed.

2. Study Area and Data

2.1. Study Area

The LP is located in the upper and central reaches of the Yellow River between 33°43′ to 41°16′N and 100°54′ to 114°33′E, and it occupies a total area of 64 × 104 km^2 (Figure 1). The climate for most of the region is

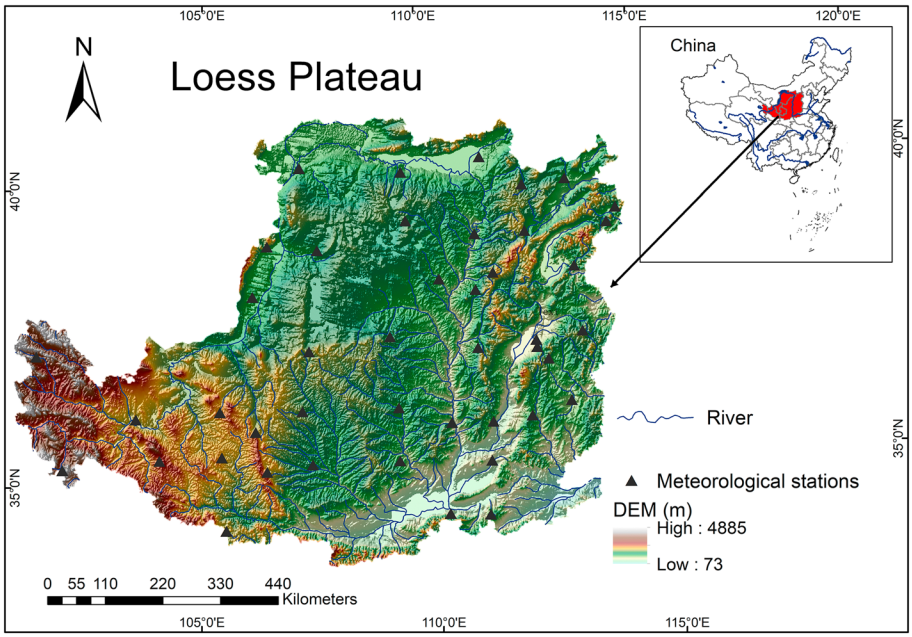

Figure 1. Location and topography map of Loess Plateau and meteorological stations.

subhumid and semiarid, and annual precipitation ranges from 150 to 800 mm (increasing from northwest to southeast). The LP has an uneven precipitation distribution, strong evaporation, and poor vegetation coverage, and it thus suffers from severe water shortages, serious soil erosion, and land degradation (Shi & Shao, 2000). The annual mean temperature ranges from 3.6 °C in the northwest to 14.3 °C in the southeast, and it has increased by 0.22 °C per decade over the past 60 years for the whole LP (Wang et al., 2017). Precipitation across the LP has shown a slightly decreasing trend of −3.17 mm per decade over the past six decades (Zhou et al., 2015). In addition, 80–91% of the precipitation occurs during the rainfall season between May and October; therefore, when the drought level is determined for these six months, it is representative of the drought level for the whole year.

Although 8.5% of China's total population live in this region (the total population is approximately 86 million), the water resources of the LP account for only 2% of the country's total water resources. In addition, the water utilization ratio of the major rivers is up to 70%, which far exceeds the internationally recognized water utilization threshold of 40% (Gao et al., 2009). Furthermore, according to the Yellow River Water Resources Bulletin, human water consumption increased by 86% on the LP from the 1980s to 2010, in line with rapid social economic development (Gao et al., 2017; Wang et al., 2017).

2.2. Data

In this study, gridded daily precipitation and maximum temperature data from the HadGEM2-ES climate model under historical (1985 to 2005) and two RCPs (i.e., RCP4.5 and RCP8.5 for 2036–2095) are applied to the RegCM (RegCM4.4) and the PRECIS (PRECIS2.0) model to generate high-resolution projections. Reliability of high-resolution regional climate projections are influenced by many factors such as the RCMs themselves and the driving forces from GCMs. In addition, it is noteworthy that with complex terrain, only a limited number of GCMs perform well in LP area. In the case of limited conditions for running RCMs and limited options for GCM data which can appropriately simulate the precipitation and temperature in this area, it is particularly important to select the appropriate GCM data to drive the RCM models. Based on previous research works, the outputs from HadGEM2-ES are applied to drive the RegCM and PRECIS in our study because HadGEM2-ES performs well in simulating both temperature and precipitation in China (Wang & Chen, 2014). HadGEM2-ES outputs are available from the Program for Climate Model Diagnosis and Intercomparison (http://www-pcmdi.llnl.gov). Thereafter, downscaled high-resolution climate change scenarios (at horizontal resolutions of approximately 25 km) from the RegCM and PRECIS RCMs are extracted. The projections from RegCM and PRECIS are corrected through the bias correction

Table 1
Detailed Statistical Description of Data Sets

	HadGEM-ES			
	PRECIS	RegCM	Observation	Usage
Time 1	1986–1995		1986–1995	Develop bias-correction models
Time 2	1996–2004		1996–2004	Model validation
Time 3	2036–2095		1971–2016	Comparative studies

procedure to enhance the accuracy of climate projections for further characterization of the occurrence of drought with hot extremes over PL under climate change.

The observed daily maximum temperature and precipitation data for 44 meteorological stations across the LP (Figure 1) were collected from the National Meteorological Information Center (http://data.cma.cn/), covering the period between 1971 and 2016. For the reason that there are fewer missing observed data of all stations in the period of 1986–2004, and it is also the latest period of historical outputs from the climate model (data are incomplete in 2005), data for the period 1986 to 2004 were used to conduct the bias correction and validation analyses for daily maximum temperature and monthly precipitation. The first 10-year (1986–1995) data of maximum temperature and precipitation were used to develop the bias-correction models, and the remaining nine-year data (1996–2004) were applied to conduct model validation (checking the bias-corrected results). The precipitation in the region has shown an insignificant decreasing trend over the past six decades (Zhou et al., 2015). The KS test of precipitation from May to October for periods of 1986–1995 and 1996–2004 shows that the p values of all stations are all greater than 0.05, which also indicate that there is no obvious difference in precipitation between the two periods in the LP. The T_{max} from May to October in 1996–2004 is significantly higher than that in 1986–2004 (increased by an average of 0.58°). The p values of only four stations are greater than 0.05, which means that T_{max} of two periods are significantly different and can fully validate the performance of bias correction method. Data for the entire time period (1971–2016) were employed to make a comparative study with future scenarios. Detailed descriptions of the data usage for each time period are shown in Table 1.

3. Method

Figure 2 illustrates the hot drought probabilistic recognition (HDPR) system. The HDPR system mainly consists of four modules: (i) a dynamic downscaling process for HadGEM2-ES outputs, (ii) a bias correction process for daily maximum temperature (T_{max}) and monthly precipitation, (iii) selection of the most appropriate marginal distributions and copulas for TX90p and SPI, and (iv) a joint disaster risk inference (hot drought identification) under projected climate. In detail, modules (i) and module (ii) aim to improve the quality of simulation data for future years; module (iii) is proposed to construct the reliable joint risk identification model for the risk inference module (iv), which reveals changes in projected future joint risks.

3.1. Copula Concept

As a multivariate statistical analysis method, copulas are employed to model the dependence structure between correlated random variables (Chen et al., 2017). In detail, copulas are multivariate distribution functions with marginal distributions that are uniform on the interval [0, 1] According to Sklar's theorem (Nelsen, 2006; Sklar, 1959), for an n-dimensional distribution function, F, with univariate marginals F_1, ... , F_n, a multivariate copula function, C, exists that can be expressed as

$$F(x_1,\ x_2,...,x_n) = C(F_1(x_1),\ F_2(x_2),...,F_n(x_n)) \quad (1)$$

where $x_1, x_2,... x_n$ are observed values of random variables $X_1, X_2, ... , X_n$, $F_1(x_1)$, $F_2(x_2)$, ..., and F_n (x_n) refer to the CDFs of random vector $(X_1, X_2, ... , X_n)$. If all these marginal distributions are continuous and differentiable, then a single copula function exists, which can be written as (Nelsen, 2006; Sraj et al., 2015)

$$C(u_1,u_2,...,u_n) = F\left(F_1^{-1}(u_1),F_2^{-1}(u_2),...,F_n^{-1}(u_n)\right) \quad (2)$$

where $u_1 = F_1(x_1)$, $u_2 = F_2(x_2 ...)$,... and, $u_n = F_n$ (x_n). More details about the theoretical background and characteristics of different copula families are shown in Nelsen (2006).

A large number of copulas families are widely used in risk analysis, including Archimedean, elliptical, and extreme value copulas. Of these, Archimedean copulas are quite attractive because their mathematical tractability (which can be expressed by a single-argument generator function) and can capture varieties of dependence structures with several desirable properties, such as symmetry and associativity (Fan et al., 2015).

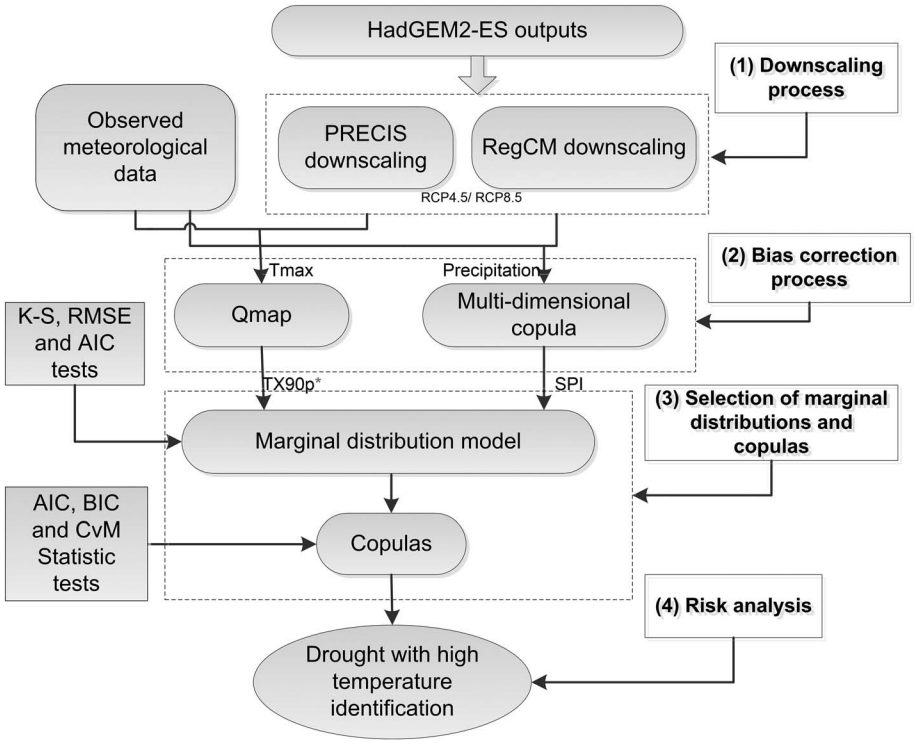

Figure 2. Hot drought probabilistic recognition system, which mainly consists of four modules (1) to (4).

Rank-based statistical tests for bivariate symmetry of SPI and Tx90p are conducted for all stations under both historical and two future scenarios (44 stations × 3 scenarios) in this study (see Genest et al., 2012; Hofert et al., 2018). It is found that most of the stations (42 of historical, 41 of RCP4.5, and 42 of RCP8.5) have obvious symmetry in SPI and Tx90p for both historical and future scenarios, copulas with symmetric structure are beneficial to drought events with high temperature studies. With a large variety of copulas belong to this family, the Archimedean copula family can be applied when the correlation among variables is positive or negative. The benefit of the elliptical family over the Archimedean is that elliptical copulas can specify different levels of correlation between the marginal distributions (Berentsen et al., 2014). As is know that extreme copula is beneficial for the analysis of extreme situations, however, the goal of this research is to model the entire distribution to capture events with high return frequencies and not only the extremes. Hence, extreme value copulas might not be appropriate in this study.

In the present study, the Frank, Clayton, and Gumbel copulas (in the Archimedean family) and the Gaussian, Student's *t* copulas (most commonly used elliptical copulas) are selected as candidate models to construct the bias correction and risk assessment models. The *t*-copula and some of the Archimedean copulas can perform well in capturing tail dependency (e.g., Clayton copula for lower tail dependence and Gumbel copula for upper tail dependence; see Schölzel & Friederichs, 2008). The Frank and Gaussian copulas are comprehensive in capturing the full range of dependence between two random variables (Bhat & Eluru, 2009), which also fulfill the needs of modeling the entire distribution to capture events with high return frequencies and extremes. Some basic properties for the three chosen Archimedean copulas are presented in Table 2.

The CDF of a *d*-dimensional Gaussian copula is given by

$$\begin{aligned} C(u_1, u_2, ..., u_d; \Sigma) &= \Phi_\Sigma\left(\Phi^{-1}(u_1), ..., \Phi^{-1}(u_d)\right) \\ &= \int_{-\infty}^{\Phi^{-1}(u_1)} ... \int_{-\infty}^{\Phi^{-1}(u_d)} \frac{1}{2(\pi)^{d/2}|\Sigma|^{1/2}} \exp\left(-\frac{1}{2} w^T \Sigma^{-1} w\right) dw \end{aligned} \tag{3}$$

where Φ_Σ represents the multivariate normal distribution with a correlation matrix, Σ, Φ^{-1} is the inverse of

Table 2
Basic Properties of Applied Bivariate Archimedean Copulas

Copula	$C(u, v; \theta)$	$\tau = 1 + 4\int_0^1 \frac{\varphi(t)}{\varphi'(t)} dt$	Generator ($\varphi(t)$)	θ
Frank	$-\frac{1}{\theta}\ln\left\{1+\frac{(e^{-\theta u}-1)(e^{-\theta v}-1)}{e^{-\theta}-1}\right\}$	$1-\frac{4}{\theta}[D_1(-\theta)-1]$[a]	$-\ln\left[\frac{e^{-\theta t}-1}{e^{-\theta}-1}\right]$	$(-\infty, +\infty)\backslash\{0\}$
Clayton	$(u_1{}^{-\theta}+u_2{}^{-\theta}-1)^{-1/\theta}$	$\frac{2}{\theta+2}$	$(t^{-\theta}-1)/\theta$	$(0, +\infty)$
Gumbel-Hougaard	$\exp\{-[(-\ln u)^{\theta}+(-\ln v)^{\theta}]^{1/\theta}\}$	$1-\theta^{-1}$	$(-\ln t)^{\theta}$	$[1, +\infty)$

[a]D_1 is the first-order Debye function, for any positive integer k, $D_k(x) = \frac{k}{x^k}\int_0^k \frac{t^k}{e^t-1} dt$.

the univariate normal distribution, and w symbolizes the integrand variable matrix. The distribution function of the d-dimensional t copula is given by

$$C(u_1, u_2, ..., u_d; \Sigma, v) = \Phi_{\Sigma,v}\left(\Phi^{-1}(u_1), ..., \Phi^{-1}(u_d)\right) = \int_{-\infty}^{\Phi^{-1}(u_1)} \cdots \int_{-\infty}^{\Phi^{-1}(u_d)} \frac{\Gamma\left(\frac{v+d}{2}\right)}{\Gamma\left(\frac{v}{2}\right)} \frac{1}{(\pi v)^{d/2}|\Sigma|^{1/2}} \left(1+\frac{w^T\Sigma^{-1}w}{v}\right)^{-\frac{v+d}{2}} dw \quad (4)$$

where $\Phi_{\Sigma,v}$ represents the standard multivariate Student's t distribution with a correlation matrix, Σ, and v degrees of freedom, and Φ^{-1} is the inverse of the univariate t distribution.

The parameters for copulas are obtained through a maximum likelihood estimation (Fan et al., 2015; Shih & Louis, 1995). To evaluate the performance and select the best fitted copulas, the goodness-of-fit statistics test is conducted based on Akaike's information criteria (AIC; Akaike, 1974) and Cramér von Mises statistics (Genest et al., 2009). The AIC can be obtained as follows (Karmakar & Simonovic, 2009):

$$\mathrm{AIC} = N \times \log(\mathrm{MSE}) + 2k \quad (5)$$

where N is the sample size, MSE is the mean square error, and k is the number of parameters, which describes the effective degree of freedom.

3.2. Bias Correction Model for Precipitation

In this study, the Kendall's correlation coefficients between observed precipitation and PRECIC/RegCM simulations at all stations range from 0.32/0.34 to 0.60/0.62 in the period of 1986–2004. The copula functions are applied to establish a multivariate probabilistic model between observed precipitation and the projection from two RCMs. The established model is then used to conduct bias correction for simulated precipitation in projected future periods. The detailed theoretical calculation process is as follows: once the copula function (mentioned above) is established, the joint probability density function $f(x_1, x_2, \ldots, x_n)$ corresponding to the joint CDF $F(x_1, x_2, \ldots, x_n)$ can be obtained by a product of the marginal densities and copula probability density $c(u_1, u_2, \ldots, u_n)$ (Fan et al., 2017),

$$f(x_1, x_2, ..., x_n) = \frac{\partial^n C(u_1, u_2, ..., u_n)}{\partial u_1 \partial u_2 ... \partial u_n} \frac{\partial u_1}{\partial x_1}\frac{\partial u_2}{\partial x_2} \cdots \frac{\partial u_n}{\partial x_n} = c(u_1, u_2, ..., u_n) \prod_{i=1}^{n} f_i(x_i), \quad (6)$$

where $f_i(x_i)$ is the probability density function of $F_i(x_i)$.

The parameters of multidimensional copula functions are usually difficult to calculate directly, and an alternative scheme that decomposes a multivariate density into multiple two-dimensional copula functions is always implemented (Aas et al., 2009). For equation (6) above, $f(x_1, x_2, \ldots, x_n)$ can be decomposed as

$$f(x_1, x_2, ..., x_n) = f_1(x_1) f_{2|1}(x_2|x_1) \cdot f_{3|1,2}(x_3|x_1, x_2) \cdot \ldots \cdot f_{n|1,2,\ldots,n-1}(x_n|x_2, ..., x_{n-1}) \quad (7)$$

where $f_{j\,|\,1,2,\ldots,j-1}(x_j|x_2, \ldots, x_{j-1})\ j = 2,3,..., n$ represents the conditional probability density distribution and is abbreviated as $f(x_j|x_2, \ldots, x_{j-1})$ in the following sections.

According to the general definition of the conditional density and the joint density in equation (6), the conditional density is derived by

$$f(x_n|x_2,...,x_{n-1}) = \frac{f(x_1,x_2,...,x_n)}{f(x_1,x_2,...,x_{n-1})} = f_n(x_n)\frac{c(F_1(x_1),\ F_2(x_2),...,F_n(x_n))}{c(F_1(x_1),\ F_2(x_2),...,F_n(x_{n-1}))} \tag{8}$$

In the case of three-variable situation, as in our study, the precipitation of observation and two RCMs are used as random variables: Under the assumption that there exist complex correlations among the variables, possible decomposition of the probability density function $f(x_1,x_2,x_3)$ and the conditional density functions can be expressed as equations (9)–(11),

$$f(x_1,x_2,x_3) = f_1(x_1)f(x_2|x_1)f(x_3|x_1,x_2) \tag{9}$$

$$f(x_2|x_1) = \frac{f(x_1,x_2)}{f(x_1)} = f_2(x_2)c(F_1(x_1),\ F_2(x_2)) \tag{10}$$

$$\begin{aligned} f(x_3|x_1,x_2) &= \frac{f(x_2,x_3|x_1)c_{2,3|1}(F(x_2|x_1),F(x_3|x_1))f(x_2|x_1)f(x_3|x_1)}{f(x_2|x_1)\qquad\qquad f(x_2|x_1)} \\ &= c_{2,3|1}(F(x_2|x_1),F(x_3|x_1))f(x_3|x_1) \\ &= c_{2,3|1}(F(x_2|x_1),F(x_3|x_1))c(F_1(x_1),\ F_3(x_3))f(x_3) \end{aligned} \tag{11}$$

In practical calculation, the calculation process can be simplified by using conditional independence, which means when X_2 and X_3 are assumed to be conditionally independent given X_1. This assumption may reduce the number of levels of the pair-copula decomposition, and hence simplify the construction (see Aas et al., 2009). This would be particular meaningful when a large number of RCMs are used. Based on the probability integral transform (Rosenblatt, 2011), dependent variables can be converted into a new set of variables that are independent and uniform. If we assume that $X = (X_1, X_2,..., X_n)$ is a random vector with marginal distributions $F_i(x_i)$ and $F_{i\,|\,1,2,\,\ldots\,,i-1}(x_i|\,x_1,\ \ldots\,,x_{i-1})\,(i = 1,2,...,n)$ denotes the conditional distributions, according to the probability integral transform theory,

$$\begin{cases} w_1 = F_1(x_1) = u_1 \\ w_2 = F_{2|1}(x_2|x_1) = C_{2|1}(u_2|u_1), \\ w_3 = F_{3|1,2}(x_3|x_1,x_2) = C_{3|1,2}(u_3|u_1,u_2), \\ \cdots = \cdots \\ w_n = F_{n|1,2,...,(n-1)}(x_n|x_1,\cdots,x_{n-1}) = C_{n|1,2...,(n-1)}(u_n|u_1,u_2,...,u_{n-1}) \end{cases} \tag{12}$$

where w_1, w_2, ..., w_n are independent and uniform over [0, 1]. When applying an inverse Rosenblatt transform, T_c, to the uniform sample, it can be formulated as

$$\begin{cases} u_1 = w_1 \\ u_2 = C^{-1}_{2|1}(w_2|u_1), \\ u_3 = C^{-1}_{3|1,2}(w_3|u_1,u_2), \\ \cdots = \cdots \\ u_n = C^{-1}_{n|1,2,...,(n-1)}(w_n|u_1,\cdots,u_{n-1}) \end{cases} . \tag{13}$$

According to the marginal distribution of X_i, the values of x_i corresponding to simulation values of u_i can then be obtained.

3.3. Univariate and Joint Return Periods

Once the marginal distributions of SPI and TX90p are characterized, the univariate return periods of droughts and high temperature regarding only one variable are also derived under the baseline and two RCP scenarios. Return periods of droughts are defined based on the nonexceedance probabilities of certain SPI values. While the return period of high temperature at a certain level is defined based on the exceedance probabilities of a certain TX90p (Li et al., 2015). The relevant calculation formulas are as follows:

Table 3
Comparison of Statistical Test Results for Marginal Distribution of Precipitation at Taiyuan Station

Precipitation	Marginal Distribution	K-S Test		RMSE	AIC
		T	*P* Value		
Observation	GMM	0.0957	0.2221	0.0332	−813.4
	GEV	0.0963	0.2161	0.0496	−714.7
PRECIS	GMM	0.0683	0.6291	0.0234	−896.7
	LN	0.0768	0.4779	0.0388	−775.7
RegCM	GMM	0.0539	0.8766	0.0206	−927.5
	Weibull	0.0609	0.7652	0.0286	−848.6

$$T_{\mathrm{SPI}} = \frac{1}{F_{\mathrm{SPI}}(x_1)} \tag{14}$$

$$T_{\mathrm{TX90p}} = \frac{1}{1-F_{\mathrm{TX90p}}(x_2)} \tag{15}$$

where T_{SPI} represent the return periods for a SPI smaller than or equal to a certain value, x_1, while T_{TX90p} represents return periods for a TX90p greater than or equal to certain values of x_2. In addition, F_{SPI} and F_{TX90p} are the cumulative probability distribution functions of SPI and TX90p, respectively. If appropriate copulas are specified to reflect the joint probabilistic characteristics between SPI and TX90p, the joint return periods which defined as the frequency of simultaneous occurrence of two events can be formulated as

$$\begin{aligned} T^{AND}_{X_1,X_2} &= \frac{E(L)}{P(X_1 \le x_1, X_2 > x_2)} = \frac{E(L)}{P(X_1 \le x) - P(X_1 \le x_1, X_2 \le x_2)} \\ &= \frac{E(L)}{F_{X_1}(x_1) - C(F_{X_1}(x_1), F_{X_2}(x_2))} \end{aligned} \tag{16}$$

where $T^{AND}_{X_1,X_2}$ denotes the return period when $X_1 \le x_1$ and $X_2 \ge x_2$, and in the present study, X_1 and X_2 represent SPI and TX90p, respectively. $E(L)$ denotes the average interarrival time between recorded events, the annual index values of SPI and TX90p are used in this paper, so $E(L)$ equals 1 here.

4. Analysis of Results

4.1. Case Study of Various Distributions

Taiyuan station (37°22′N and 112°21′E) in the eastern LP is used as a case to illustrate the computation procedure. It is necessary to consider a marginal distribution model during the process of precipitation bias correction and when establishing the bivariate distribution procedure for SPI and TX90p. In the fitting of marginal distribution models and copulas for SPI and TX90p, entire data sets for both history (1971–2016) and future (2036–2095) are used. The candidate marginal distribution models considered in this study are the Gaussian mixture model (GMM), gamma, lognormal, Pearson type III, Log Pearson type III, generalized extreme value, and Weibull distributions. These models are selected because they are widely used for fitting the distributions of precipitation, drought, and high temperature indicators (Angelidis et al., 2012; Hao et al., 2017; Wang et al., 2014; Yusof et al., 2013). The Expectation-Maximization algorithm (EM; Sondergaard & Lermusiaux, 2013) is applied to generate parameters for the GMM distribution, and the parameters for other marginal distributions and copulas are obtained through a maximum likelihood estimation (Fan et al., 2015; Shih & Louis, 1995). Furthermore, the root-mean-square error, AIC (Akaike, 1974), and Kolomogorov-Smirnov tests are used to test and select the most appropriate marginal distribution (Fan et al., 2015).

The distribution of precipitation is always complicated. Based on the goodness-of-fit statistics test, it is found that with the exception of the GMM, candidate marginal distribution models are generally poor in fitting the distribution of precipitation in this region (the *p* values obtained by the Kolomogorov-Smirnov test at some stations are less than 0.05). The finite GMM can theoretically be very close to any continuous distribution if a sufficient number of components are properly given (Fan et al., 2016). Therefore, the GMM is used to model precipitation in this area, and to evaluate its performance, goodness-of-fit tests results of the GMM are compared with the best fitted ones of six other distributions at Taiyuan station. Table 3 shows the AIC, root-mean-square error, and Kolomogorov-Smirnov test values of the GMM and other selected distributions for monthly precipitation at Taiyuan station. The *p* value for the GMM is larger than the other distributions, which shows goodness of fit, and it can thus be concluded that the GMM is the most appropriate for modeling the distribution of observed monthly precipitation and simulations obtained from two RCMs. Figure 3 illustrates a comparison between the performances of the GMM and the other most suitable distributions at Taiyuan station. The GMM-based CDFs and probability density functions for the marginal distributions of different precipitation data show better agreements with the empirical distributions than that of other theoretical distributions.

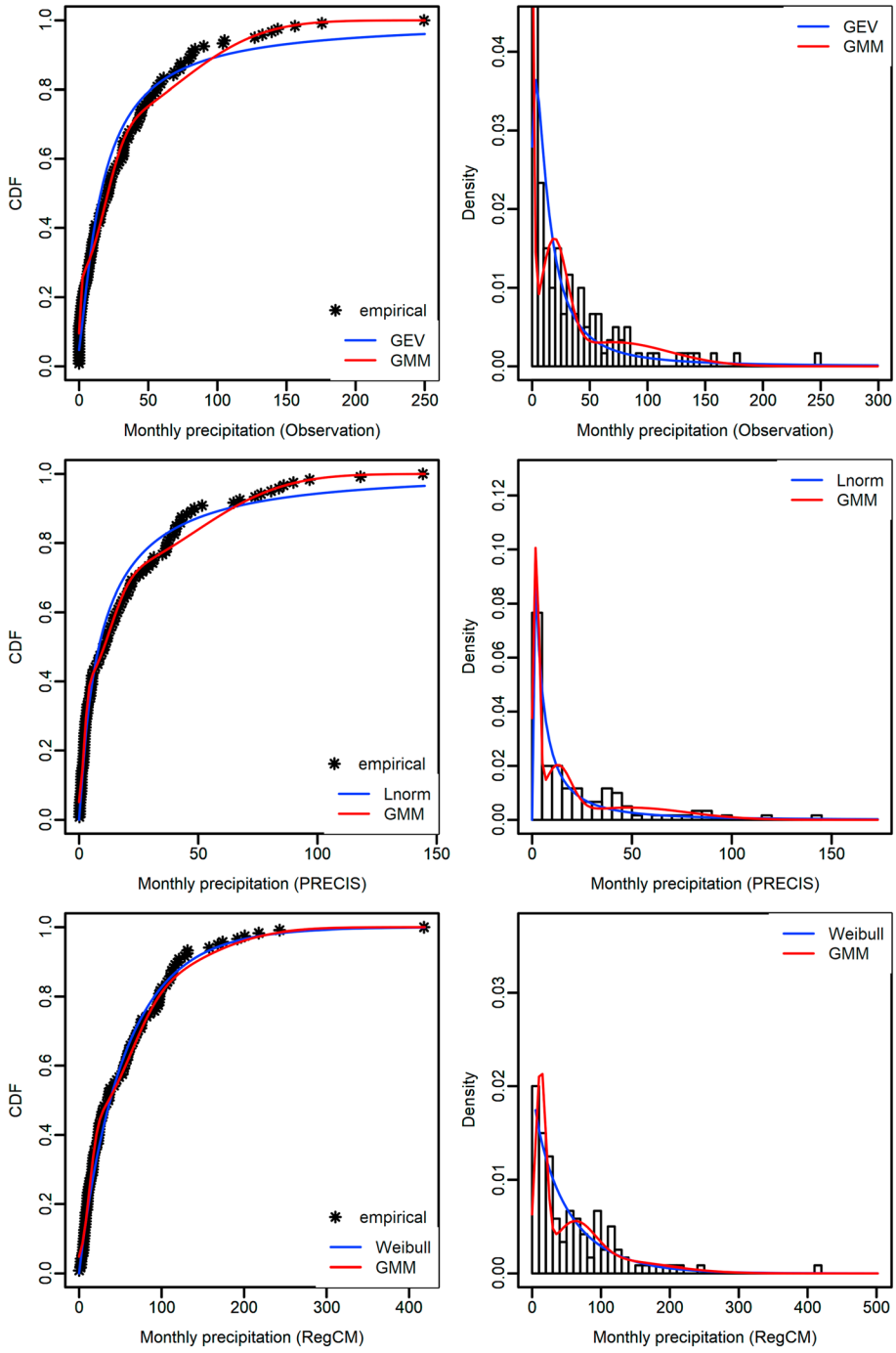

Figure 3. Comparison of GMM and other probability density estimates with theoretical frequency at Taiyuan station.

Although the GMM distribution is able to quantify the distributions of SPI and TX90p, it should be noticed that the GMM is computationally expensive and has more parameters (which may bring more uncertainties) than other marginal distribution models. When there exist other models that satisfy the goodness-of-fit tests, we tend to choose other marginal distributions rather than the GMM. After calculating the marginal distribution, it was found that the SPI values of all stations in the LP were more in line with Pearson type III or extreme distribution, while the TX90p values were more consistent with the Gamma or Pearson type III distribution. When the marginal distributions of the two indicators for all stations were determined, the calculation of the copula functions could then be conducted. Using Taiyuan station as an example, the SPI and

Table 4
Performance of Different Copulas for Joint Distributions Between SPI and TX90p at Taiyuan Station

	Copulas	Parameter	Tau	AIC	CvM[a]	*P* Value
History	Gaussian	−0.413	−0.27	−6.75	0.014	0.79
RCP4.5	Student *t*	−0.49, 4.69	−0.32	−15.34	0.342	0.86
RCP8.5	Gaussian	−0.231	−0.15	−1.28	0.006	0.75

[a]The Cramér-von Mises statistic proposed by Genest et al. (2009), with *p* value larger than 0.05 indicating satisfactory performance.

TX90p of historical and future simulation data were found to be negatively correlated (Kendall's tau was negative); therefore, the copula function was selected and the Gumbel copula function was excluded. Table 4 shows the parameters used when selected copulas and the corresponding statistical test indexes for historical and two projected future scenarios, and Figure 4 illustrates the cumulative distributions of the best fitted marginal distributions and bivariate probability distribution of SPI and TX90p for the historical period.

4.2. Bias Correction Results

In this study, the quantile mapping method (Q_{map}; Piani, Haerter, & Coppola, 2010, Piani, Weedon, et al., 2010) is used to correct the deviation of the daily maximum temperature of downscaled outputs from PRECIS and RegCM models. For the PRECIS model, the coefficient of determination (R^2) on a daily time scale for the validation period (1996–2004) range from 0.63 to 0.79 for the 44 stations, with an average of 0.734, whereas those for the corrected RegCM outputs fluctuate from 0.55 to 0.81, with an average of 0.715. The correction results for all stations for both the PRECIS and RegCM models on a monthly time scale have an averaged R^2 value higher than 0.95; therefore, the correction results of the two models can meet the general needs of climate change analysis. In addition, according to our research characteristics, the 0.9 quartile values of daily maximum temperature for each station were also verified, and bias correction performances for daily maximum temperature at the 90th percentile threshold for observations and RCMs simulations at 44 stations are shown in Figure 5. With a smaller root-mean-square error value of 0.477 and a higher R^2 value of 0.995, the PRECIS model was chosen to

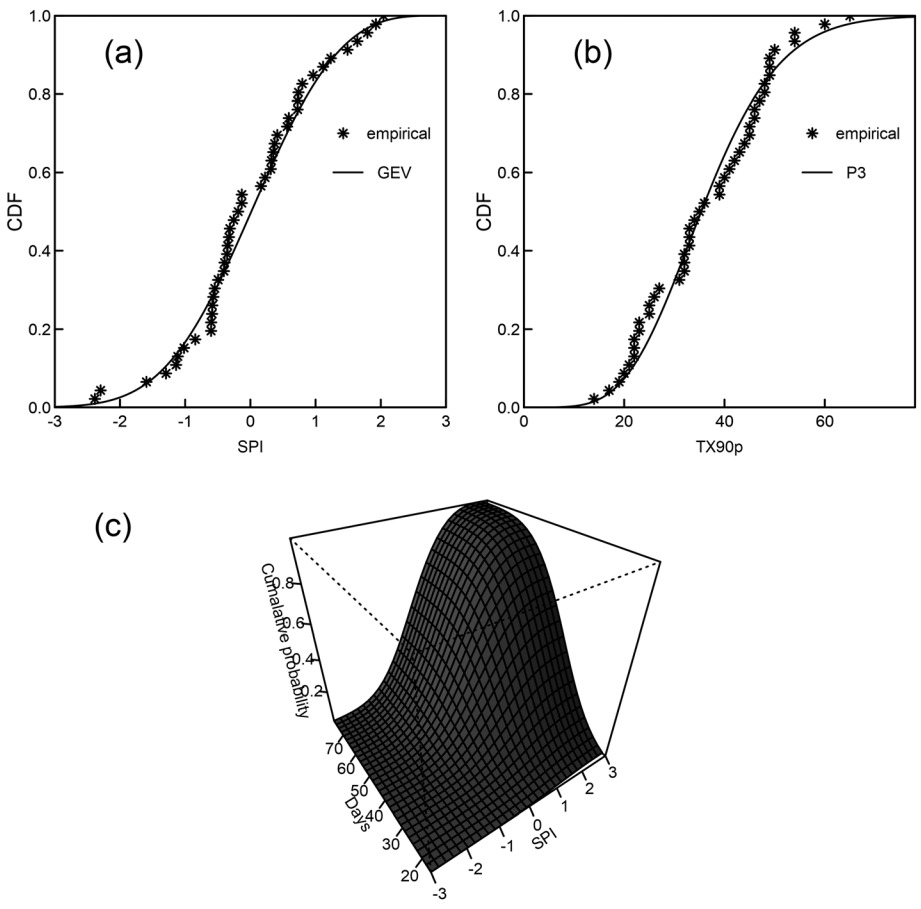

Figure 4. Marginal CDFs and 3-D surface plot of bivariate CDF for Taiyuan station. (a and b) Generated marginal CDFs of SPI and TX90p compared with theoretical distributions. (c) Joint CDF of SPI and TX90p.

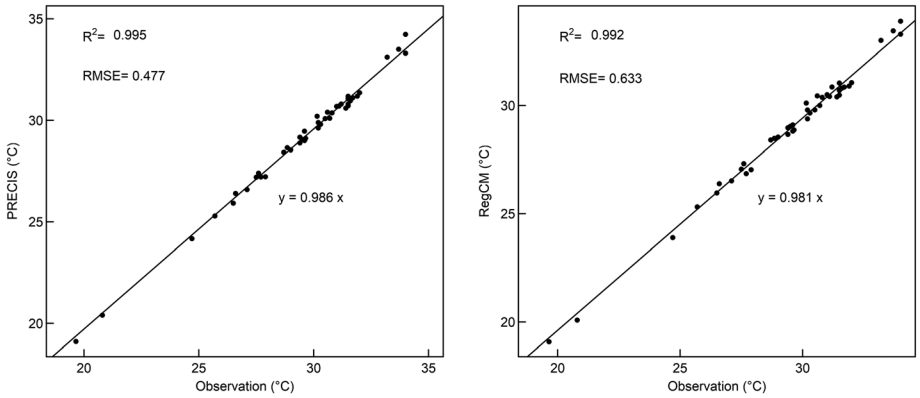

Figure 5. Comparisons of bias correction performance for daily maximum temperature from two RCMs at 44 stations. Black points show daily maximum temperature at the 90th percentile threshold for observations and RCM simulations.

analyze future daily maximum temperature changes of the LP. It is noteworthy that the predicted temperature is overall slightly lower than the observed temperature. This is because the T_{max} in 1986–2005 is significantly higher than that in 1996–2004, and the RCM simulations have not fully captured this change.

Monthly precipitation projections from PRICIS and RegCM models were jointly corrected by the proposed multidimensional copula model. Moreover, the model's performance was then compared to the Q_{map} method, which is a commonly used bias correction method. Figure 6a compares the corrected monthly mean precipitation averaged for all stations using the different methods (for selected six months), and it is evident

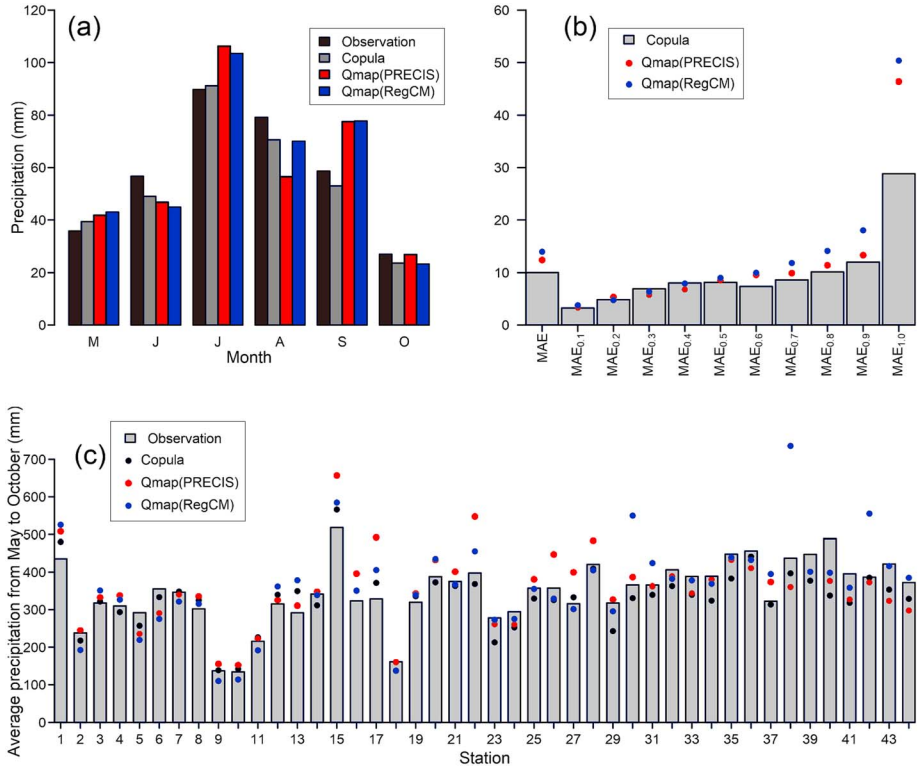

Figure 6. Comparisons between performances of different methods used for precipitation bias correction (for selected six months). (a) Monthly mean precipitation averaged over all stations. (b) Total mean absolute error (MAE) and MAE for specific probability intervals ($MAE_{0.1}$, $MAE_{0.2}$, ..., $MAE_{1.0}$) averaged over all stations. (c) Annual average rainfall from different methods for all stations.

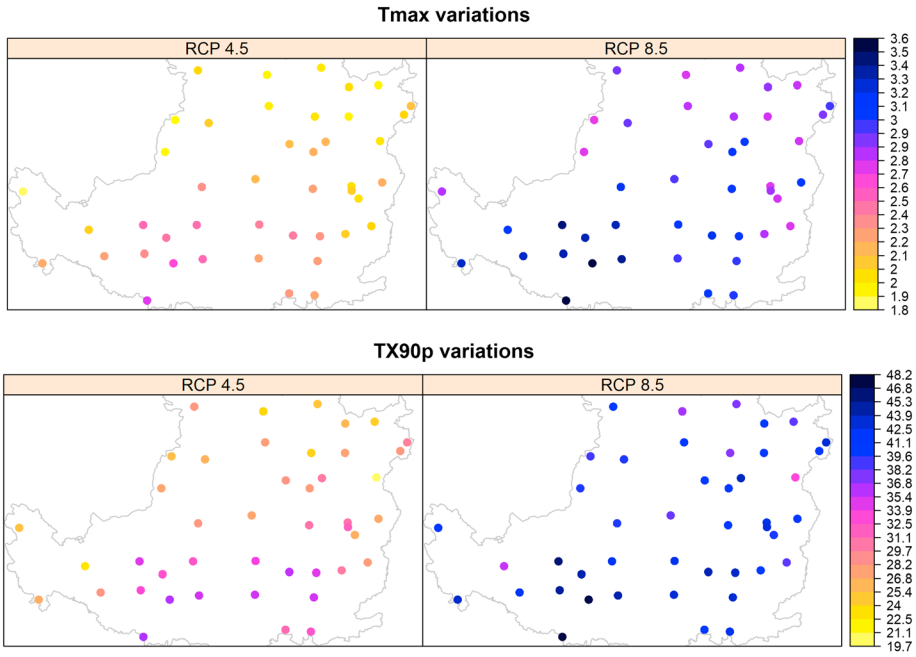

Figure 7. Mean daily maximum temperature and TX90p changes of selected six months over 44 weather stations under projected scenarios of RCP 4.5 and RCP 8.5 relative to historical situations.

that the corrected results obtained by the multidimensional copula model outperform those obtained by the Q_{map} method. Based on the mean absolute error (MAE; Gudmundsson et al., 2012), a global quantitative evaluation was conducted to further assess the methods' performances with respect to specific properties. The total MAE, together with a set of MAE scores for uniformly spaced probability intervals ($MAE_{0.1}$, $MAE_{0.2}$, ..., $MAE_{1.0}$) averaged over all stations were used to conduct more specific quantitative evaluations (Figure 6b; also for selected six months). It is evident that the total MAE value obtained by the multidimensional copula model is smaller than that from Q_{map} method. In addition, the values of MAEs for specific probability intervals calculated from the proposed model are similar to or obviously smaller than (especially for wetter months of $MAE_{0.6–1.0}$) those obtained from the Q_{map} method. Verification results of mean precipitation from May to October for all stations are shown in Figure 6c. It can be seen that the corrected precipitation (by Q_{map} method) deviates significantly from observations at some stations, while it shows no serious deviations between observations and corrected values obtained from the multidimensional copula model. The performance of multidimensional copula model is slightly inferior to that of the Q_{map} method at only a few stations. However, the combined results show that the performance of multidimensional copula model is relatively more stable than that of the Q_{map} method.

After conducting the bias correction process, a simple statistical calculation was conducted to determine changes in precipitation and daily maximum temperature (T_{max}) made between historical and projected future scenarios. The average daily mean maximum temperature from May to October at 44 meteorological stations shows an increasing trend from 1.8 to 2.7 °C for the RCP 4.5 scenario and 2.7 to 3.6 °C for the RCP 8.5 scenario in relation to historical situations, and the average mean daily mean maximum temperature at 44 meteorological stations increases by 2.15 °C and 3.03 °C for the RCP 4.5 scenario and RCP 8.5 scenario, respectively. The corresponding TX90p values show an average increase ranging from 19.7 to 36.3 for the RCP 4.5 scenario and 33.6 to 48.2 for the RCP 8.5 scenario. Figure 7 shows changes in the mean daily maximum temperature and TX90p from May to October at each weather station under the two projected future scenarios relative to historical situations.

For stations with the most precipitation reduction, annual mean precipitation from May to October would decrease by 154 and 153 mm for the RCP 4.5 scenario and RCP 8.5 scenario, respectively. While the annual average precipitation (from May to October) may increase by 297 mm for the RCP 4.5 scenario and 316 mm for the RCP 8.5 scenario at stations with the most precipitation increment. Mean precipitation for the 44

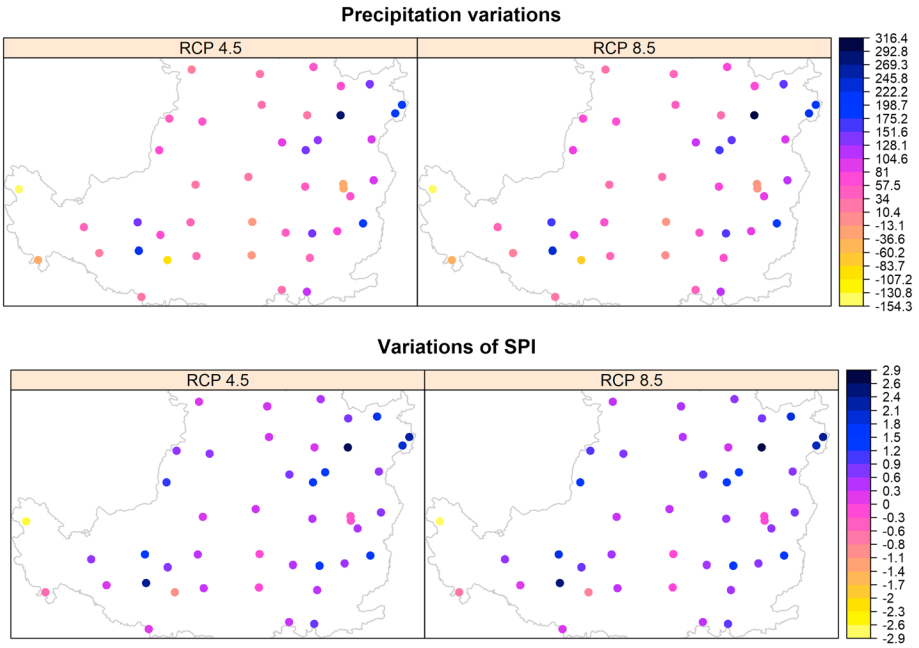

Figure 8. Mean precipitation and SPI changes for selected six months over 44 weather stations under projected scenarios of RCP 4.5 and RCP 8.5 relative to historical situations.

meteorological stations over the six months shows average increases of 61 and 75 mm for the RCP 4.5 scenario and RCP 8.5 scenario, respectively. The corresponding SPI values fluctuate from −2.8 to 2.8 for the RCP 4.5 scenario and −2.9 to 2.9 for the RCP 8.5 scenario. Figure 8 shows the detailed changes in precipitation and SPI for six months at each weather station under the two projected future scenarios relative to historical situations. Precipitation for the whole LP shows an obvious increased trend in both future scenarios, while there are severe precipitation decreases in some areas, and thus, the severity of drought could be aggravated with the increase of temperature.

4.3. Spatial Distributions of Univariate and Joint Return Periods

Using the best fitted marginal distribution, the SPI and TX90p values for specific return periods can be calculated according to equations (14) and (15), respectively. Spatial distributions of SPI and TX90p values for historical and two RCP scenarios corresponding to a return period of 50 years (the most serious case) in the LP are shown in Figure 9. The first row of Figure 9 presents a comparison of SPI between historical and two RCP scenarios, while the second row shows the variation in TX90p. As can be seen from the figure, the spatial distributions of SPI in the two future scenarios are similar, and the values are larger than those in the historical period in most parts of the LP. Severe drought events in future scenarios are mainly detected in the southwest and in a small part of south-central LP. The 50-year return period of TX90p values for the entire LP in the two future scenarios are obviously larger than the historical ones, especially for the RCP 8.5 scenario. The average TX90p of the 44 meteorological stations for the RCP 4.5 scenario and RCP 8.5 scenario increases by 32.3 and 55.7, respectively, compared to the corresponding historical value of 63.3. The risk of long-term high temperatures in the future may therefore increase significantly. Considering the 50-year return period values of SPI and TX90p under two future scenarios, it can be qualitatively judged that drought occurring with continuous high temperature will happen frequently in the south-central and southwest parts of the LP in future.. In order to quantitatively calculate the combined risk of the two indicators at each station (see equation (16)), it is necessary to set different risk level combinations of the two indicators.

Two levels for TX90p and SPI indices are set, respectively, and joint return periods under four combination schemes are then calculated. According to the historical and future 50-year return period of TX90p in Figure 9, the levels of 60 and 90 days are set for TX90p. The drought severity is classified using SPI

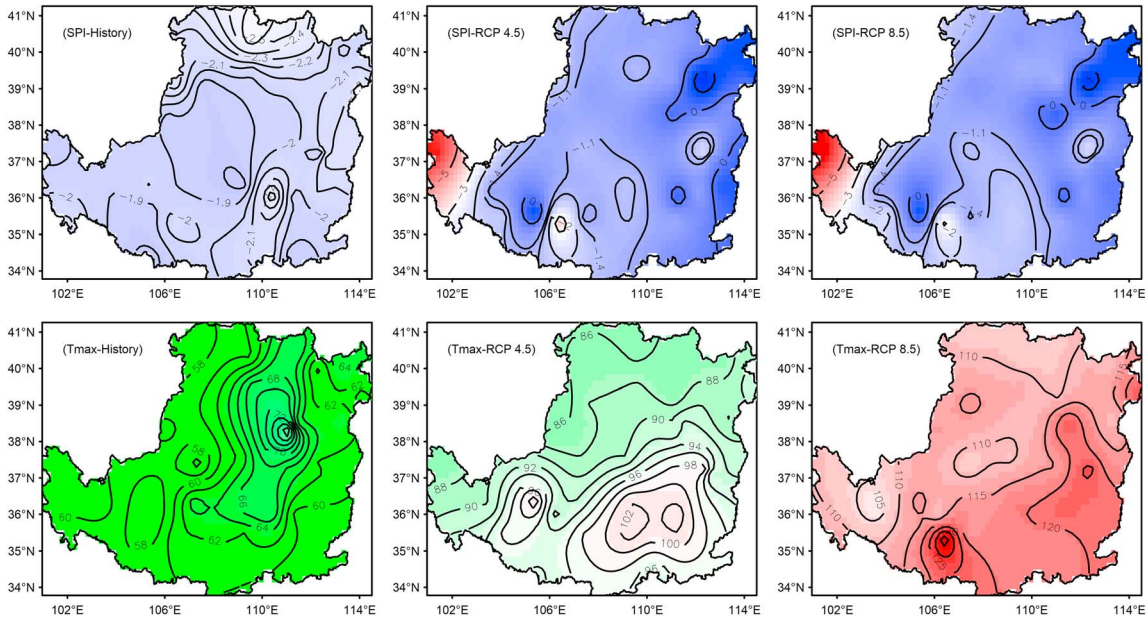

Figure 9. Comparison of 50-year return period values for SPI and TX90p between historical and two RCP scenarios.

index according to recommendations by National Climate Center of China (2017). We classify drought conditions based on SPI using two thresholds of −0.5 and −1, which are used for distinguishing mild drought from nondrought and moderate drought from mild drought, respectively. The precipitation corresponding to SPI = −0.5 is lower than almost 68% of the historical precipitation series in this area. When SPI is equal to −1, the corresponding precipitation is lower than about 83% of the historical precipitation series. The average precipitation corresponding to SPI values of −0.5 and −1 for all stations in May–October would be 306.7 and 267.8 mm, respectively. Four situations are then considered for the analysis of joint return periods: (i) SPI is −0.5 with TX90p of 60 and considered to be mild drought with mid-long-term high temperatures in this study, (ii) SPI is −1 with TX90p of 60 and is considered to be moderate drought with mid-long-term high temperatures, (iii) SPI is −0.5 with TX90p of 90 and is considered to be mild drought with long-term high temperatures, and (iv) SPI is −1 with TX90p of 90 and is considered to be moderate drought with long-term high temperatures. For the scenarios (i) and (ii), a comparison between historical and future joint return periods is conducted. While for scenarios (iii) and (iv), the joint return periods are analyzed only for future scenarios (TX90p = 90 can hardly happen in history).

Figure 10 shows stations with joint return periods of less than 100 years (red bubbles) and their corresponding return period values for the first two scenarios. The size of the red bubble corresponding to each station is inversely proportional to the magnitude of the joint return period. From Figure 10, it is evident that the number of stations with joint return periods of less than 100 under the two future scenarios is less than the historical situation, and the return periods are also significantly smaller (with bigger bubbles in Figures 10b, 10c, 10b*, and 10c*). This indicates that future drought conditions at the stations shown in the figure are more severe for the first two scenarios. The return periods at some stations in the southwest and south-central regions are even less than 10 years, which means that there may be a higher frequency of drought with mid-long-term high temperatures. The return periods of drought accompanied by long-term high temperatures (for the last two situations) are shown in Figure 11, which only shows stations with joint return periods of less than 100 years. The number of stations likely to suffer from drought with long-term high temperatures is significantly lower than for the first two conditions, which are mainly located in the southern part of the LP. There are more stations with joint return periods less than 100 years in the RCP 8.5 scenario than in the RCP 4.5 scenario. The recurrence periods of RCP 8.5 scenario for the displayed stations are mostly less than that of RCP4.5 scenario, which means that these stations may experience a higher frequency of the extreme cases.

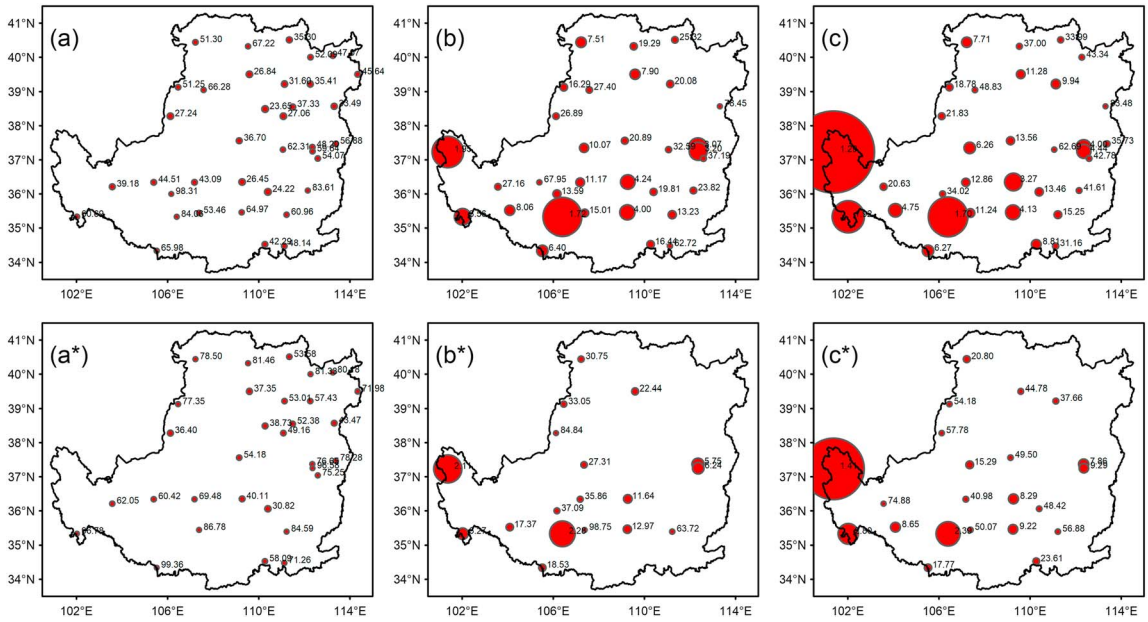

Figure 10. Stations with joint return periods of less than 100 years and corresponding return period values under different scenarios. (a–c) Joint return periods with SPI = −0.5 and TX90p = 60 under historical, RCP4.5, and RCP8.5 scenarios, respectively. (a*–c*) Joint return periods with SPI = −1 and TX90p = 60 under historical, RCP4.5, and RCP8.5 scenarios, respectively.

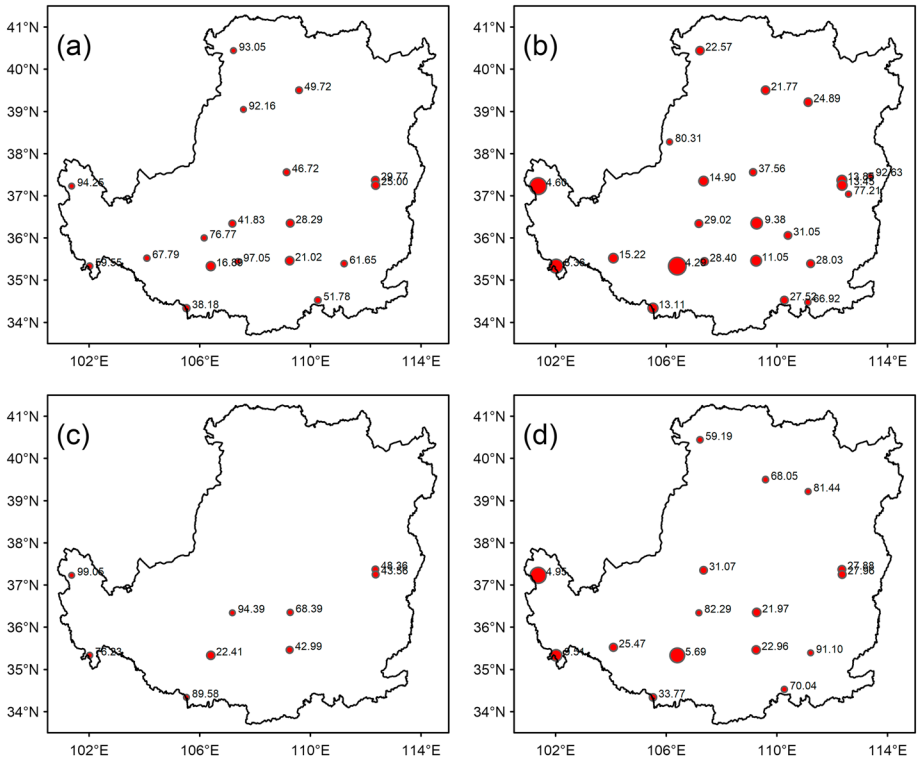

Figure 11. Stations with joint return periods of less than 100 years and corresponding return period values under different scenarios. (a and b) Joint return periods with SPI = −0.5 and TX90p = 90 under RCP4.5 and RCP8.5 scenarios, respectively. (c and d) Joint return periods with SPI = −1 and TX90p = 90 under RCP4.5 and RCP8.5 scenarios, respectively.

5. Discussion and Conclusions

Drought is a major natural disaster occurring on the Loess Plateau, and a warming climate trend is anticipated to exacerbate drought events. It is important to analyze droughts that occur simultaneously with heat waves to enable water resource planning and management. In this study, a HDPR system was developed to investigate the potential future climate change impacts on droughts and hot extremes in the Loess Plateau. The entire modeling system can be divided into four modules that function independently from each other but are interconnected during the modeling process. In detail, the model system was applied to the Loess Plateau using the following process: (i) daily maximum temperature and precipitation under RCP 4.5 and RCP 8.5 scenarios from HadGEM2-ES model were downscaled by the RCMs of PRECIS and RegCM; (ii) high-resolution downscaled T_{max} and precipitation were bias corrected by Q_{map} and proposed multidimensional copula model, respectively; (iii) TX90p and SPI were extracted from the historical and bias corrected future (2036–2095) T_{max} and precipitation for 44 stations, and a number of marginal distribution functions and copulas were investigated to characterize the marginal and joint behavior of TX90p and SPI; and (iv) according to the univariate probabilistic models and copula-based models, the univariate and bivariate frequency were calculated for both .historical and future scenarios.

The performance of multidimensional copula model was generally better than the commonly used Q_{map} method for correcting monthly precipitation at different stations over the LP. After the bias correction process, the spatial distributions of univariate and bivariate return periods for SPI and TX90p were then analyzed. The results indicated an inconsistency between identified drought accompanied by high temperature for different stations in different regions and time periods. The spatial distributions of the 50-year return period for SPI and TX90p detected severe drought mainly in the southwest and south-central LP in future scenarios, while the TX90p values for the entire LP using the two future scenarios were dramatically larger than those of historical data. The joint return periods of SPI and TX90p were then investigated considering four situations. A comparison of historical situation and two future scenarios showed that fewer stations in the future may suffer from severe drought with long-term hot extremes, but some may experience a higher frequency of drought with long-term high temperatures, particularly some stations in the southwest and south-central regions of the LP, with an average recurrence period of less than 10 years. Under the combined action of the two kinds of disaster in these areas where drought with long-term hot extremes are likely to occur more frequently, local industry, agricultural production, and even human health can be seriously affected. It should be noticed that only two RCMs are used in this study; the reliance of projections may be limited but would be enhanced when more accurate RCM projections are integrated into the proposed modeling framework. From a planning perspective, the findings of this paper are also important to local decision makers and practitioners.

Acknowledgments
This research was supported by the National Key Research and Development Plan (2016YFA0601502), the Natural Sciences Foundation (51520105013, 51679087), the 111 Program (B14008), the Natural Science and Engineering Research Council of Canada, and the Fundamental Research Funds for the Central Universities (2016XS89). The observed temperature and precipitation data are collected and available at the National Meteorological Information Center (http://data.cma.cn/). The RCM simulations are available at Climate Change Data Portal (http://chinaccdp.org/).

References

Aas, K., Czado, C., Frigessi, A., & Bakken, H. (2009). Pair-copula constructions of multiple dependence. *Insurance Mathematics & Economics*, *44*(2), 182–198. https://doi.org/10.1016/j.insmatheco.2007.02.001

Akaike, H. (1974). A new look at the statistical model identification. *IEEE Transactions on Automatic Control*, *19*(6), 716–723. https://doi.org/10.1109/TAC.1974.1100705

Angelidis, P., Maris, F., Kotsovinos, N., & Hrissanthou, V. (2012). Computation of drought index SPI with alternative distribution functions. *Water Resources Management*, *26*(9), 2453–2473. https://doi.org/10.1007/s11269-012-0026-0

Asadi Zarch, M. A., Sivakumar, B., & Sharma, A. (2015). Droughts in a warming climate: A global assessment of Standardized Precipitation Index (SPI) and Reconnaissance Drought Index (RDI). *Journal of Hydrology*, *526*, 183–195. https://doi.org/10.1016/j.jhydrol.2014.09.071

Bandyopadhyay, N., Bhuiyan, C., & Saha, A. K. (2016). Heat waves, temperature extremes and their impacts on monsoon rainfall and meteorological drought in Gujarat, India. *Natural Hazards*, *82*(1), 1–22.

Bates, B. C., Kundzewicz, Z. W., Wu, S., & Palutikof, S. (2008). *Climate change and water. Technical Paper of the Intergovernmental Panel on Climate Change* (p. 210). Geneva: IPCC Secretariat.

Berentsen, G. D., StøVe, B., TjøStheim, D., & Nordbø, T. (2014). Recognizing and visualizing copulas: An approach using local Gaussian approximation. *Insurance: Mathematics and Economics*, *57*, 90–103.

Bhat, C. R., & Eluru, N. (2009). A copula-based approach to accommodate residential self-selection effects in travel behavior modeling. *Transportation Research Part B Methodological*, *43*(7), 749–765. https://doi.org/10.1016/j.trb.2009.02.001

Burke, E. J., Brown, S. J., & Christidis, N. (2006). Modeling the recent evolution of global drought and projections for the twenty-first century with the Hadley Centre Climate Model. *Journal of Hydrometeorology*, *7*(5), 1113–1125. https://doi.org/10.1175/JHM544.1

Chen, F., Huang, G. H., Fan, Y. R., & Chen, J. P. (2017). A copula-based fuzzy chance-constrained programming model and its application to electric power generation systems planning. *Applied Energy*, *187*, 291–309. https://doi.org/10.1016/j.apenergy.2016.11.065

Dubrovsky, M., Svoboda, M. D., Trnka, M., Hayes, M. J., Wilhite, D. A., Zalud, Z., & Hlavinka, P. (2009). Application of relative drought indices in assessing climate-change impacts on drought conditions in Czechia. *Theoretical & Applied Climatology*, *96*(1-2), 155–171. https://doi.org/10.1007/s00704-008-0020-x

Fan, Y. R., Huang, G. H., Baetz, B. W., Li, Y. P., & Huang, K. (2017). Development of a copula-based particle filter (CopPF) approach for hydrologic data assimilation under consideration of parameter interdependence. *Water Resources Research*, *53*, 4850–4875. https://doi.org/10.1002/2016WR020144

Fan, Y. R., Huang, W. W., Huang, G. H., Huang, K., Li, Y. P., & Kong, X. M. (2015). Bivariate hydrologic risk analysis based on a coupled entropy-copula method for the Xiangxi River in the Three Gorges reservoir area, China. *Theoretical & Applied Climatology*, *125*(1-2), 381–397.

Fan, Y. R., Huang, W. W., Huang, G. H., Li, Y. P., Huang, K., & Li, Z. (2016). Hydrologic risk analysis in the Yangtze River basin through coupling Gaussian mixtures into copulas. *Advances in Water Resources*, *88*, 170–185. https://doi.org/10.1016/j.advwatres.2015.12.017

Food and Agricultural Organisation of United nations (FAO) (2002). *Report of FAO-CRIDA Expert Group Consultation on Farming System and Best Practices for Drought-prone Areas of Asia and the Pacific Region*, published by. Hyderabad, India: Central Research Institute for Dry land Agriculture.

Gao, X., Zhao, Q., Zhao, X., Wu, P., Pan, W., Gao, X. D., & Sun, M. (2017). Temporal and spatial evolution of the Standardized Precipitation Evapotranspiration Index (SPEI) in the loess plateau under climate change from 2001 to 2050. *Science of the Total Environment*, *595*, 191–200. https://doi.org/10.1016/j.scitotenv.2017.03.226

Gao, Z. L., Li, Y. H., Xu, J., Wang, Z. Z., Zhao, J., Guo, W., et al. (2009). Research on eco-construction and control measures of soil and water loss in the Loess Plateau (in Chinese). *Science Technology and Industry*, *9*, 1–12.

Genest, C., Nešlehová, J., & Quessy, J. F. (2012). Tests of symmetry for bivariate copulas. *Annals of the Institute of Statistical Mathematics*, *64*(4), 811–834. https://doi.org/10.1007/s10463-011-0337-6

Genest, C., Rémillard, B., & Beaudoin, D. (2009). Goodness-of-fit tests for copulas: A review and a power study. *Insurance Mathematics & Economics*, *44*(2), 199–213. https://doi.org/10.1016/j.insmatheco.2007.10.005

Gudmundsson, L., Bremnes, J. B., Haugen, J. E., & Engenskaugen, T. (2012). Technical note: Downscaling RCM precipitation to the station scale using statistical transformations—A comparison of methods. *Hydrology & Earth System Sciences Discussions*, *9*(5), 6185–6201. https://doi.org/10.5194/hessd-9-6185-2012

Guttman, N. B. (1998). Comparing the palmer drought index and the standardized precipitation index. *Journal of the American Water Resources Association*, *34*(1), 113–121. https://doi.org/10.1111/j.1752-1688.1998.tb05964.x

Hao, Z., Hao, F., Singh, V. P., & Ouyang, W. (2017). Quantitative risk assessment of the effects of drought on extreme temperature in eastern China. *Journal of Geophysical Research: Atmospheres*, *122*, 9050–9059. https://doi.org/10.1002/2017JD027030

Heim, R. R. (2002). A review of twentieth-century drought indices used in the United States. *Bulletin of the American Meteorological Society*, *83*(8), 1149–1166. https://doi.org/10.1175/1520-0477-83.8.1149

Hofert, M., Kojadinovic, I., Machler, M., & Yan, J. (2018). *Elements of copula modeling with R*. Berlin, Germany: Springer International Publishing AG. https://doi.org/10.1007/978-3-319-89635-9

Huang, J., Zhai, J., Tong, J., Wang, Y., Li, X., Wang, R., et al. (2018). Analysis of future drought characteristics in China using the regional climate model CCLM. *Climate Dynamics*, *50*(1-2), 1–19.

IPCC (2007). *Climate change 2007: The physical science basis. Contribution of Working Group I to the Fourth Assessment Report of the Intergovernmental Panel on Climate Change*. Cambridge, UK and New York: Cambridge University Press.

Kallis, G. (2008). Droughts. *Annual Review of Environment and Resources*, *33*(1), 85–118. https://doi.org/10.1146/annurev.environ.33.081307.123117

Karl, T. R., Nicholls, N., & Ghazi, A. (1999). CLIVAR/GCOS/WMO workshop on indices and indicators for climate extremes: Workshop summary. *Climate Change*, *42*(1), 3–7. https://doi.org/10.1023/A:1005491526870

Karmakar, S., & Simonovic, S. P. (2009). Bivariate flood frequency analysis. Part 2: A copula-based approach with mixed marginal distributions. *Journal of Flood Risk Management*, *2*(1), 32–44.

Keyantash, J., & Dracup, J. A. (2002). The quantification of drought: an evaluation of drought indices. *Bulletin of the American Meteorological Society*, *83*(8), 1167–1180. https://doi.org/10.1175/1520-0477-83.8.1167

Li, Z., Huang, G. H., Fan, Y. R., & Xu, J. L. (2015). Hydrologic risk analysis for nonstationary streamflow records under uncertainty. *Journal of Environmental Informatics*, *26*(1), 41–51.

Li, Z., Zheng, F. L., Liu, W. Z., & Flanagan, D. C. (2010). Spatial distribution and temporal trends of extreme temperature and precipitation events on the loess plateau of China during 1961–2007. *Quaternary International*, *226*(1), 92–100.

Liu, Z., Wang, Y., Shao, M., Jia, X., & Li, X. (2016). Spatiotemporal analysis of multiscalar drought characteristics across the loess plateau of China. *Journal of Hydrology*, *534*, 281–299. https://doi.org/10.1016/j.jhydrol.2016.01.003

Masters J. (2013). Top ten global weather events of 2012. Weather Underground. https://www.wunderground.com/blog/JeffMasters/top-ten-global-weather-events-of-2012.html (last visit: 2018-06-06)

Mazdiyasni, O., & Aghakouchak, A. (2015). Substantial increase in concurrent droughts and heatwaves in the United States. *Proceedings of the National Academy of Sciences of the United States of America*, *112*(37), 11,484–11,489. https://doi.org/10.1073/pnas.1422945112

Mekis, E., & Vincent, L. A. (2006). Changes in daily and extreme temperature and precipitation indices related to droughts in Canada, 17th Conference on Applied Climatology. https://ams.confex.com/ams/13MontMet17AP/techprogram/paper_140963.htm

Mishra, A. K., & Singh, V. P. (2010). A review of drought concepts. *Journal of Hydrology*, *391*(1), 202–216. https://doi.org/10.1016/j.jhydrol.2010.07.012

Mueller, B., & Seneviratne, S. I. (2012). Hot days induced by precipitation deficits at the global scale. *Proceedings of the National Academy of Sciences of the United States of America*, *109*(31), 12,398–12,403. https://doi.org/10.1073/pnas.1204330109

National Climate Center (2017). Grades of meteorological drought. Standards Press of China. GB/T20481-2017 (pp. 3) (in Chinese).

Nelsen, R. B. (2006). *An Introduction to Copulas*. New York: Springer.

NOAA National Centers for Environmental Information (NCEI) U.S. Billion-Dollar Weather and Climate Disasters (2018). https://www.ncdc.noaa.gov/billions/events/US/2012

Osuch, M., Romanowicz, R. J., Lawrence, D., & Wong, W. K. (2016). Trends in projections of standardized precipitation indices in a future climate in Poland. *Hydrology and Earth System Sciences*, *20*(5), 1947–1969. https://doi.org/10.5194/hess-20-1947-2016

Piani, C., Haerter, J. O., & Coppola, E. (2010). Statistical bias correction for daily precipitation in regional climate models over Europe. *Theoretical & Applied Climatology*, *99*(1-2), 187–192. https://doi.org/10.1007/s00704-009-0134-9

Piani, C., Weedon, G. P., Best, M., Gomes, S. M., Viterbo, P., Hagemann, S., & Haerter, J. O. (2010). Statistical bias correction of global simulated daily precipitation and temperature for the application of hydrological models. *Journal of Hydrology*, *395*(3-4), 199–215. https://doi.org/10.1016/j.jhydrol.2010.10.024

Rosenblatt, M. (2011). Remarks on a multivariate transformation. *Annals of Mathematical Statistics*, *23*(3), 470–472. https://doi.org/10.1214/aoms/1177729394

Schölzel, C., & Friederichs, P. (2008). Multivariate non-normally distributed random variables in climate research—Introduction to the copula approach. *Nonlinear Processes in Geophysics*, *15*(5), 761–772. https://doi.org/10.5194/npg-15-761-2008

She, D., & Xia, J. (2018). Copulas-based drought characteristics analysis and risk assessment across the loess plateau of china. *Water Resources Management*, *32*(56), 1–18.

Shi, H., & Shao, M. (2000). Soil and water loss from the loess plateau in China. *Journal of Arid Environments*, *45*(1), 9–20. https://doi.org/10.1006/jare.1999.0618

Shih, J. H., & Louis, T. A. (1995). Inferences on the association parameter in copula models for bivariate survival data. *Biometrics*, *51*(4), 1384–1399. https://doi.org/10.2307/2533269

Sklar, M. (1959). *Fonctions de repartition à n dimensions et leurs marges* (Vol. 8, pp. 229–231). Paris: Publications de l'Institut de Statistique de l'Universite dé Paris.

Sondergaard, T., & Lermusiaux, P. F. J. (2013). Data assimilation with Gaussian mixture models using the dynamically orthogonal field equations. Part I: Theory Scheme. *Monthly Weather Review*, *141*(6), 1761–1785. https://doi.org/10.1175/MWR-D-11-00296.1

Sraj, M., Bezak, N., & Brilly, M. (2015). Bivariate flood frequency analysis using the copula function: A case study of the Litija station on the Sava River. *Hydrological Processes*, *29*(2), 225–238. https://doi.org/10.1002/hyp.10145

U.S. Department of Energy (2013). U.S. Energy Sector Vulnerabilities to Climate Change and Extreme Weather. US Department of Energy Report, DOE-PI-0013.

Vicente-Serrano, S. M., Beguería, S., & López-Moreno, J. I. (2010). A multiscalar drought index sensitive to global warming: the Standardized Precipitation Evapotranspiration Index. *Journal of Climate*, *23*(7), 1696–1718. https://doi.org/10.1175/2009JCLI2909.1

Vidal, J. P., & Wade, S. (2009). A multimodel assessment of future climatological droughts in the United Kingdom. *International Journal of Climatology*, *29*(14), 2056–2071. https://doi.org/10.1002/joc.1843

von Buttlar, J., Zscheischler, J., Rammig, A., Sippel, S., Reichstein, M., Knohl, A., et al. (2018). Impacts of droughts and extreme-temperature events on gross primary production and ecosystem respiration: A systematic assessment across ecosystems and climate zones. *Biogeosciences*, *15*(5), 1293–1318. https://doi.org/10.5194/bg-15-1293-2018

Wang, L., & Chen, W. (2014). A CMIP5 multimodel projection of future temperature, precipitation, and climatological drought in China. *International Journal of Climatology*, *34*(6), 2059–2078. https://doi.org/10.1002/joc.3822

Wang, S., Fu, B., Piao, S., Lü, Y., Ciais, P., Feng, X., & Wang, Y. (2017). Reduced sediment transport in the Yellow River due to anthropogenic changes. *Nature Geoscience*, *9*(1), 38–41.

Wang, Y., Fan, C., Zhang, J., Niu, T., Zhang, S., & Jiang, J. (2014). Forecast verification and visualization based on Gaussian mixture model co-estimation. *Computer Graphics Forum*, *34*(6), 1–12.

World Bank (2003). *India, Financing Rapid Onset Natura Disaster Losses in India: A Risk Management Approach, Report No. 26844-IN*. Washington, DC: World Bank.

Wu, J., Miao, C., Zheng, H., Duan, Q., Lei, X., & Li, H. (2018). Meteorological and hydrological drought on the loess plateau, China: Evolutionary characteristics, impact, and propagation. *Journal of Geophysical Research: Atmospheres*, *123*, 11,569–11,584. https://doi.org/10.1029/2018JD029145

Xu, K., Yang, D., Yang, H., Li, Z., Qin, Y., & Shen, Y. (2015). Spatio-temporal variation of drought in China during 1961–2012: A climatic perspective. *Journal of Hydrology*, *526*, 253–264. https://doi.org/10.1016/j.jhydrol.2014.09.047

Yusof, F., Hui-Mean, F., Suhaila, J., & Yusof, Z. (2013). Characterisation of drought properties with bivariate copula analysis. *Water Resources Management*, *27*(12), 4183–4207. https://doi.org/10.1007/s11269-013-0402-4

Zaitchik, B. F., Macalady, A. K., Bonneau, L. R., & Smith, R. B. (2006). Europe's 2003 heat wave: A satellite view of impacts and land-atmosphere feedbacks. *International Journal of Climatology*, *26*(6), 743–769. https://doi.org/10.1002/joc.1280

Zhang, B., Wu, P., Zhao, X., Wang, Y., Wang, J., & Shi, Y. (2012). Drought variation trends in different subregions of the Chinese loess plateau over the past four decades. *Agricultural Water Management*, *115*(115), 167–177. https://doi.org/10.1016/j.agwat.2012.09.004

Zhang, L., & Zhou, T. (2015). Drought over East Asia: A review. *Journal of Climate*, *28*(8), 3375–3399. https://doi.org/10.1175/JCLI-D-14-00259.1

Zhou, J., Liang, Z., Liu, Y., Guo, H., He, D., & Zhao, L. (2015). Six-decade temporal change and seasonal decomposition of climate variables in lake Dianchi watershed (China): Stable trend or abrupt shift? *Theoretical & Applied Climatology*, *119*(1-2), 181–191. https://doi.org/10.1007/s00704-014-1098-y

Zhou, X., Huang, G., Wang, X., Fan, Y., & Cheng, G. (2017). A coupled dynamical-copula downscaling approach for temperature projections over the Canadian Prairies. *Climate Dynamics*, *51*(7-8), 2413–2431.

Zscheischler, J., & Seneviratne, S. I. (2017). Dependence of drivers affects risks associated with compound events. *Science Advances*, *3*(6), e1700263. https://doi.org/10.1126/sciadv.1700263